Electrochemical Behavior and Corrosion Inhibition of Zinc Electrode in Solutions of $(NH_4)_2SO_4$ Containing Ce(IV) Ions

W. A. M. Hussein [1], E. M. Attia [1,] I.M.Ghayad[2] and W. A. M. Ghanem [2]

[1] Chemistry Department, Faculty of Science (for Girls), Al- Azhar University, Nasr City, Cairo, Egypt
[2] Central Metallurgical Research and Development Institute (CMRDI)
wallaahmed@yahoo.com

Abstract: The corrosion behavior of Zn in $(NH_4)_2SO_4$ solutions in absence and in the presence of Ce(IV) ions and the effect of adding two different surfactants as corrosion inhibitors was studied using potentiodynamic, potentiostatic and cyclic voltammetry techniques complemented with scanning electron microscopy and electron dispersion X-ray analysis (SEM/EDX). In $(NH_4)_2SO_4$ solutions, the E/I curves indicated active/passive transition peak in the anodic region which become more active by increasing sulfate ion concentration. Increasing the scan rate has no effect on the corrosion rate while the combined effect of sulfate and Ce(IV) ions accelerate the corrosion rate than that caused by $(NH_4)_2SO_4$ alone. This complemented by potentiostatic polarization technique which indicated that the stability of the oxide film is affected by the applied potentials. The addition of sodium salt of N-(2-hydroxy-3- sulfopropyl)-5- stearyl -1,3,4-triazole-2-thione (17T-HSP) and potassium salt of N-(carboxymethyl)- 5- stearyl -1,3,4-triazole-2-thione (17T-CM) lead in all cases to inhibition of the corrosion process but with low values. Surfactant 17T-CM inhibits the anodic reaction only, while 17T-HSP depressing both the anodic and cathodic reactions. The difference in molecular structure contributes to the different adsorption mechanism. Langmuir and Freundlich adsorption isotherms were tested for fitting the experimental data of the studied compounds.
[W. A. M. Hussein, E. M. Attia, I.M.Ghayad and W. A. M. Ghanem. **Electrochemical Behavior and Corrosion Inhibition of Zinc Electrode in Solutions of $(NH_4)_2SO_4$ Containing Ce(IV) Ions.** *Researcher* 2014;6(1):1-11]. (ISSN: 1553-9865). http://www.sciencepub.net/researcher. 1

Keywords: Zinc; Corrosion; inhibition; polarization; Surfactant.

1. Introduction

Owing to its unique merits, including no toxicity, high specific energy (0.82 Ah g^{-1}), rich resource and low cost, zinc has been widely used as anode material in many applications [1]. It is extensively used as a coating for carbon steel because of its good corrosion resistance [2-4]. The property which gives zinc this valuable resistance is its ability to form a protective layer consisting zinc oxide and hydroxide or various basic salts depending on the nature of the environment [5, 6]. In view of the widespread use of zinc, as metallic sheet or zinc coatings, it was desirable to study its corrosion behavior in the wide variety of environments.

Some researchers have studied the influence of different salts particularly Na_2SO_4 on the corrosion of zinc [2-9]. In contrary, only very little work has been done concerning corrosion of Zn by $(NH_4)_2SO_4$ [7-9]. Researchers also have studied the combined effect of two salts on the corrosion of zinc. It was stated that the combined effect of NaCl and NH_4Cl on the corrosion of zinc is greater than that caused by NH_4Cl and less than that caused by NaCl [2]. Also the combined effect of Na_2SO_4 and $(NH_4)_2SO_4$ is greater than that caused by $(NH_4)_2SO_4$ and less than that caused by Na_2SO_4 [7]. However, up to now, there is no report in the literature about the combination effect of $(NH_4)_2SO_4$ and $(NH_4)_4Ce(SO_4)_4.2H_2O$ which is a very safe oxidizer and one of the most nontoxic ones.

In previous studies, many inorganic and organic anions and inorganic cations have been investigated as inhibitors for corrosion of zinc in sulfate solution by polarization measurements and surface analyses. Among them $Cr_2O_7^{2-}$, CrO_4^{2-}, WO_4^{2-} and MoO_4^{2-} ions are noticeable inhibitors for both general and pitting zinc corrosion [10, 11]. However, some of organic additives are expensive and some others are toxic. Most of them are often reported to be used individually [12].

The high affinity of organic surfactant molecules to adsorb onto interfaces is responsible for their applications in several interfacial systems. For this reason, surfactant; can be used as good corrosion inhibitors for metals [13-15]. Heterocyclic substances containing nitrogen atoms, such as triazole-type compounds are considered to be excellent corrosion inhibitors for many metals and alloys in various aggressive media [16, 17].

The present work has been undertaken to study in detail the corrosion behavior of Zn in $(NH_4)_2SO_4$ solutions over a certain range of concentrations and scan rate by potentiodynamic, potentiostatic and cyclic voltammetry measurements. The combination effect of $(NH_4)_2SO_4$ and $(NH_4)_4Ce(SO_4)_4.2H_2O$ and effect of

some triazole- type compounds on the corrosion process was also investigated.

2. Experiment

2.1. Electrode

The specimen of zinc (Johnson Matthey, purity 99.999%) with 1.54 cm^2 exposed area was made of massive cylindrical rod fixed at the end of a glass tube holder with epoxy resin. A copper wire was employed for an electrical contact. The zinc surface was polished mechanically using emery papers of Grade Nos. ranging from 220 to 1200, washed thoroughly with distilled water and degreased with acetone and finally abraded on a wet felt cloth. Then, it was immersed in the test solution.

2.2. Solutions

Both of $(NH_4)_2SO_4$ and corrosive (20mmol $(NH_4)_2SO_4$ + 25mmol $(NH_4)_4Ce(SO_4)_4.2H_2O$) solutions were prepared from a high- analytical reagent grade by dilution of a concentrated solution with bidistilled water.

2.3. Inhibitors

Both sodium salt of N-(2-hydroxy- 3-sulfopropyl)- 5-stearyl- 1,3,4-triazole-2-thione (17T-HSP) and potassium salt of N-(carboxymethyl)- 5-stearyl -1,3,4-triazole- 2-thione (17T-CM) were synthesized as according to the method in the literature [18]. The concentration range of surfactant inhibitors used was 0.5–15mmol. Figure 1 shows the molecular structure of both inhibitors.

2.4. Polarization measurement

Polarization curves of the zinc electrode were performed with electronic potentioscane volta lab 40 (PGZ 301) - Radiometer analytical. A single compartment – cylindrical three electrodes glass cell of 250 ml. capacity was used. All potentials were measured with respect to saturated calomel electrode (SCE) and a platinum sheet was used as auxiliary electrode. All measurements were performed in freshly prepared solutions at room temperature (30±2˚C). The anodic E/I curve for all solutions were swept from -1500 to +1000 mV with scan rate of 5mV/s. For cycling voltametric polarization, after attaining a steady state potential (E_{corr}), the electrode scanned at a rate of 5mV/s. Repeated runs were made for each solution, indicating a fairly good reproducibility of the curves.

2.5. SEM observation and energy dispersive X-ray analysis (EDX).

After cyclic polarization in the corrosive solutions with and without different additives at 30°C, the surface morphology of the zinc electrode was investigated under a metallurgical light microscope model (ASTM G46 Olympus Tokyo). During X- ray diffraction analysis, the X- ray beam falls on the plane of the crystal, after reflection, the beam can be detected and converted to peaks. The intensity of the peaks can give an idea about the percentage abundance of the different compounds. Prior to the observation, the zinc electrode was removed from the holder, rinsed carefully with doubly-distilled water, dried and the morphological micrographs were exposed at magnifications favored the purposes of investigation.

(17T-HSP) (17T-CM)

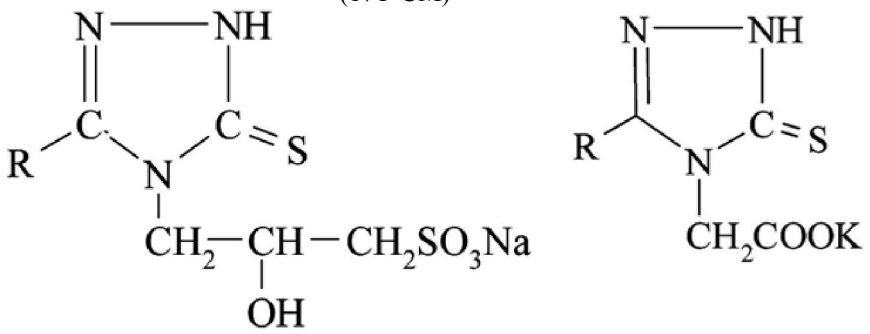

Figure 1: Model structure of the triazole- derivatives where: R = CH_3 $(CH_2)_{16}$–

The inhibition efficiency, IE %, was calculated from the following equation [18]:

$$IE\ \% = \left[1 - \frac{I_{corr}}{I^{o}_{corr}}\right] x\ 100 \qquad \ldots\ldots\ldots\ldots\ldots\ (1)$$

Where I^{o}_{corr} and I_{corr} are the corrosion current densities obtained in uninhibited and inhibited solutions. In our study all the potentiodynamic and cyclic voltametric parameters were computed by the internal computer of the Volta lab.

2. Results and Discussion

1- Effect of ammonium sulfate concentration

The potentiodynamic E/I curves of Zn electrode in $(NH_4)_2SO_4$ (Figure 2) reveal that on positive- going sweep, the cathodic current density decreases gradually and changes its sign at the corrosion potential (E_{corr}). The anodic response for concentrations ≥ 20 mmol exhibits active/passive transition represented by the anodic peak. The formation of peaks start at current density of ≈ 13.8 mA/cm^2 when the potential sweep reaching to -0.264, -0.664 and -0.760 V(SCE) for SO_4^{2-} concentrations 20, 40 and 50 mmol respectively. These peaks reach to its maximum height at potentials (E_p) -0.262, -0.662 and -0.758 V(SCE) for 20, 40 and 50mmol SO_4^{2-} with nearly the same c.d. ≈ 68.4 mA/cm^2. The peaks reach to its limiting values at -0.252, -0.652 and -0.750 V(SCE) corresponding to c.d. ≈ 14.7 mA/cm^2. Concentrations of 1 and 5mmol do not show any peaks up to potentials of +1 volt. These values illustrate that an increase in the $(NH_4)_2SO_4$ concentration, shifts the peak potential (E_p) towards more active values.

The acceleration influence of SO_4^{2-} ions could be related to its adsorption on the metal surface and subsequent participation in the active dissolution process. In concentrations 1 and 5 mmol, the amount of sulfate ions are not enough to completely cover the adsorbed surface layer and hence the active dissolution process can not start.

The observed anodic peak corresponds to the formation of zincite (ZnO) film through a dissolution-precipitation mechanism according to the following overall reaction [11]:

$$Zn + H_2O = ZnO + 2H^+ + 2e^- \quad (2)$$

The dissolution of zinc involves the formation of Zn^{2+} ions which complexes with water to form ZnO_2^{2-} ions at the electrode surface until a critical concentration is reached at which ZnO precipitates and the dissolution current drops to a limiting value I_{pass}.

In the passive region, I_{pass} decreases very rapidly as the potential are moved in the positive direction. This decrease may be due to a rapid increase in the thickness of the passive film. The electrochemical parameters illustrated in Table 1 indicate that the corrosion current increase with increasing $(NH_4)_2SO_4$ concentration.

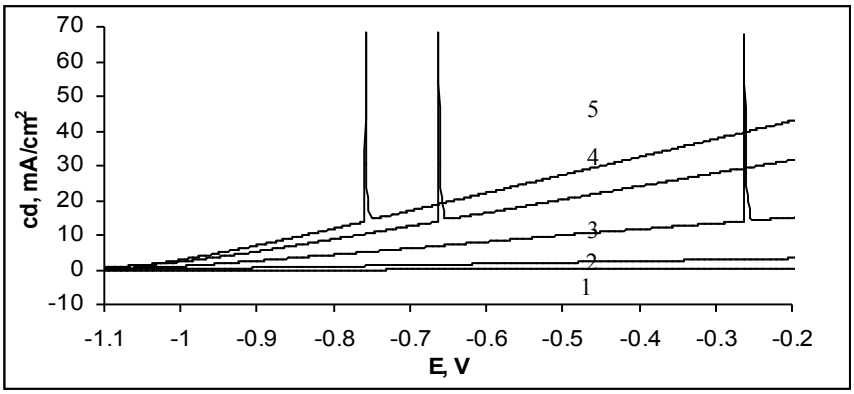

Figure 2: Potentiodynamic E/I curves of Zn electrode at 5 mVs^{-1} and 30°C in various concentrations of $(NH_4)_2SO_4$. The numbers 1,2,3,4 and 5 are corresponding to concentrations 1,5,20, 40 and 50 mmol of $(NH_4)_2SO_4$.

Table (1): Electrochemical parameters of Zn electrode at different concentrations of $(NH_4)_2SO_4$ at 5 mV/s.

Conc., mmol	E_{corr} mV	I_{corr} µA/cm^2	b_a mV/decade	b_c mV/decade	R_p Ωcm^2	C_R mm/y
1	-0734	008	298	-246	564	0.092
5	-1150	082	293	-305	619	0.961
20	-1191	127	210	-218	251	1.488
40	-1167	121	084	-225	169	1.409
50	-1171	147	102	-215	161	1.717

E_{corr}, corrosion potential i_{corr}, corrosion current density b_a, anodic Tafel slope b_c, cathodic Tafel slope Rp polarization resistance. C_R corrosion rate

When the surface of zinc is wet by $(NH_4)_2SO_4$ solution, the following reaction occurs in the anodic sites [7]:

$$Zn + 4NH_4^+ = Zn(NH_3)_4^{2+} + 4H^+ + 2e \quad (3)$$

The anodic dissolution is balanced by oxygen reduction in the cathodic areas by the following reaction:

$$O_2 + 2H_2O + 4e = 4OH^- \quad (4)$$

However in the cathodic sites, NH_4^+ will react with OH^- as follows:

$$NH_4^+ + OH^- = NH_3 + H_2O \quad (5)$$

The above reaction decreases the pH of the electrolyte, and the following reactions will take place:

$$Zn(NH_3)_4^{2+} + 2(NH_4)_2SO_4 = (NH_4)_2Zn(SO_4)_2 + 6NH_3 + 2H^+ \quad (6)$$

$$4(NH_4)_2Zn(SO_4)_2 + 11H_2O = Zn_4SO_4(OH)_6.5H_2O + 8NH_3 + 7H_2SO_4 \quad (7)$$

An ammonia-zinc complex, zinc hydroxysulfate and ZnO present on zinc surface in the presence of $(NH_4)_2SO_4$. These results are confirmed by XRD and FTIR analysis in a previous study [7].

2- Effect of Scan rate

Figure 3 illustrates the effect of scan rate (ω) on the E/I response of Zn electrode in 20 mmol $(NH_4)_2SO_4$ at 30°C. It is clear that an increase in the scan rate enhances the peak current to rise. Figure 4 show that the height of i_p fits linear i_p vs. $\omega^{1/2}$ graph. Therefore, it can be concluded that the anodic process taking place at anodic peaks corresponds to a film reaction involving mainly a diffusion-controlled process.

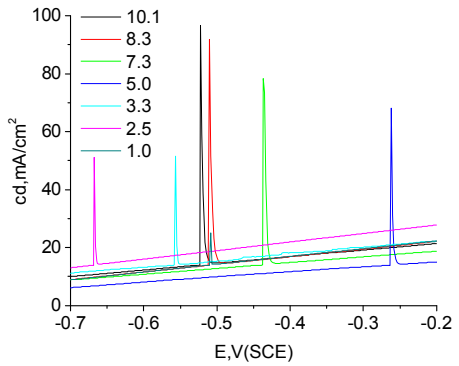

Fig 3: Potentiodynamic E/I curves of Zn in 20 mmol $(NH_4)_2SO_4$ at 30°C and different scan rates.

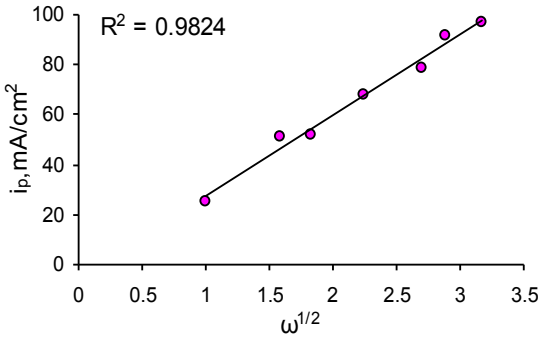

Fig 4: Dependence of i_p on $\omega^{1/2}$ in 20 mmol $(NH_4)_2SO_4$ at 30°C.

3- Additions of Ce(IV) ions

The presence of ammonium cerium (IV) sulfate in 20mmol $(NH_4)_2SO_4$ solution caused the corrosion current and corrosion rate to be shifted to more active values; this is illustrated in figure 5(a and b) and Table 2. Cyclic Voltammetric curves illustrate the appearance of a micro pit on the zinc electrode in the presence of $(NH_4)_4Ce(SO_4)_4.2H_2O$ but no growth of the pit is observed after the end of the experiment.

The OH^- ions in solution (Eq.4) are chemisorbed at the active sites forming the monovalent (ZnOH) which accelerate the active dissolution of zinc. This process is inhibited via blocking of the active sites by divalent (ZnO) which present in very low content due to its very fast transformation to other corrosion products or dissolution of the porous zinc oxide formed in the range of pH 3.8–5.8 [19-21]. Figure 5(a and b) confirm that the dissolution of Zn is strongly stimulated by the presence of ammonium cerium(IV) sulfate which increase the amount of sulfate ions in solution. On the other hand SO_4^{2-} ions has the fastest ionic mobilities in H_2O than NH_4^+ or Zn^{2+} ions (8.29, 7.63 and 5.47$\mu/10^{-8}m^2s^{-1}v^{-1}$ at 298K respectively [22]) which make it the most effective ion. Therefore on an oxide/hydroxide covered surface dissolution of zinc occurs mainly through the chemical dissolution of ZnO stimulating by the SO_4^{2-} -ions which are obviously due to the enhanced $ZnSO_4$ ion-pair formation, the stability constant is K, > 200[23].

Regarding of the presence of cerium (IV) ions, it may react with zinc metal in a manner similar to that with iron [24] as follows:

$$2Ce^{4+} + Zn \rightarrow 2Ce^{3+} + Zn^{2+} \quad (8)$$

The standard electrode potentials and the main oxidizing-reducing reactions are showed as follows:

$$Zn^{2+} + 2\,e^- \leftrightarrow Zn \ (-0.76\ V\ vs.\ NHE) \quad (9)$$

$$Ce^{4+} + e^- \leftrightarrow Ce^{3+} \ (+1.61\ V\ vs.\ NHE) \quad (10)$$

$$Ce^{3+} + 3\,e^- \leftrightarrow Ce \ (-2.48\ V\ vs.\ NHE) \quad (11)$$

The reaction of equation (8) indicated that the rare earth ion Ce^{4+} and Zn^{2+} had a depolarizing effect on the anodic reaction rate and accelerated the dissolution of base metal in solution. Furthermore, the driving force for the reduction of Ce^{4+} species is much higher than with that in the Zn^{2+}/Zn redox system. Also the standard electrode potential of Ce^{3+}/Ce is much lower than that of Zn^{2+}/Zn. So it is impossible for cerium ions to precipitate onto zinc surface [25].

Figure 6 shows surface morphology of zinc electrode after cyclic voltammetric polarization in 20mmol $(NH_4)_2SO_4$ solution in the absence and the presence of 25 mmol ammonium cerium (IV) sulfate. It is obvious that corrosion is observed in each solution but it is very serious for zinc in the presence of Ce^{+4} ions. As shown in Figure 6 b, there are many

large holes caused by corrosion at the surface of zinc electrode.

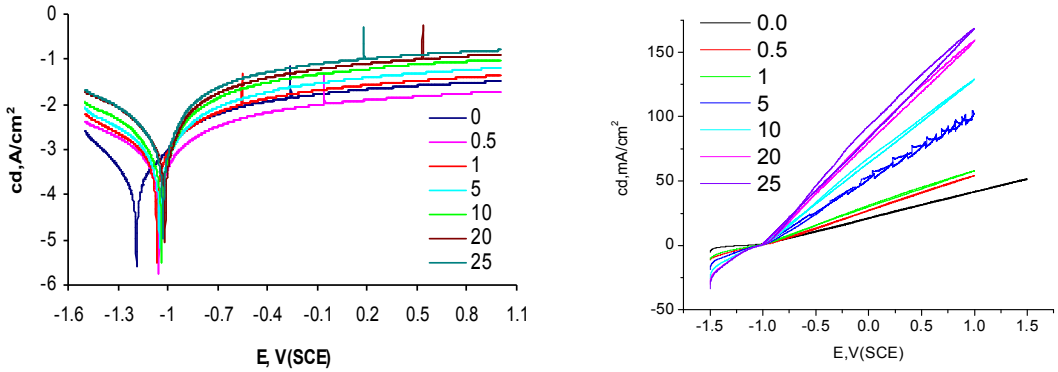

A B

Figure 5: (a) E/I plots and (b) Cyclic Voltammetric curves for Zn electrode in 20mmol $(NH_4)_2SO_4$ containing various concentrations of $(NH_4)_4Ce(SO_4)_4.2H_2O$ at 5 mVs $^{-1}$ and 30°C

Table 2: Electrochemical parameters of Zn in 20mmol ammonium sulfate solution containing different concentrations of cerium (IV) ions by potentiodynamic and cyclic voltametric techniques

	Ce^{+4} conc, mmol	E_{corr} mV	I_{corr} mA/cm^2	b_a mV/ decade	b_c mV/ decade	Rp Ωcm^2	C_R mm/y
potentiodynamic	00.0	-1191	0.1273	210	-218	251	1.488
	00.5	-1055	0.4488	346	-389	145	5.248
	01.0	-1039	0.5331	162	-247	84	6.235
	05.0	-1071	0.6072	267	-390	89	7.102
	10.0	-1052	0.6647	251	-363	99	7.775
	20.0	-1019	1.0090	179	-288	50	11.800
	25.0	-1015	1.7286	258	-419	33	20.210
Cyclic voltametric	00.0	-1153	0.1264	129	-233	207	1.5
	00.5	-1032	0.6822	165	-215	55	7.9
	01.0	-1021	0.8242	270	-319	66	9.6
	05.0	-1023	0.8690	143	-210	40	10.2
	10.0	-1056	0.8797	280	-372	61	10.3
	20.0	-1026	1.1637	172	-251	42	13.6
	25.0	-1024	1.2477	194	-281	38	14.6

E_{corr}, corrosion potential i_{corr}, corrosion current density b_a, anodic Tafel slope b_c, cathodic Tafel slope Rp polarization resistance C_R, corrosion rate.

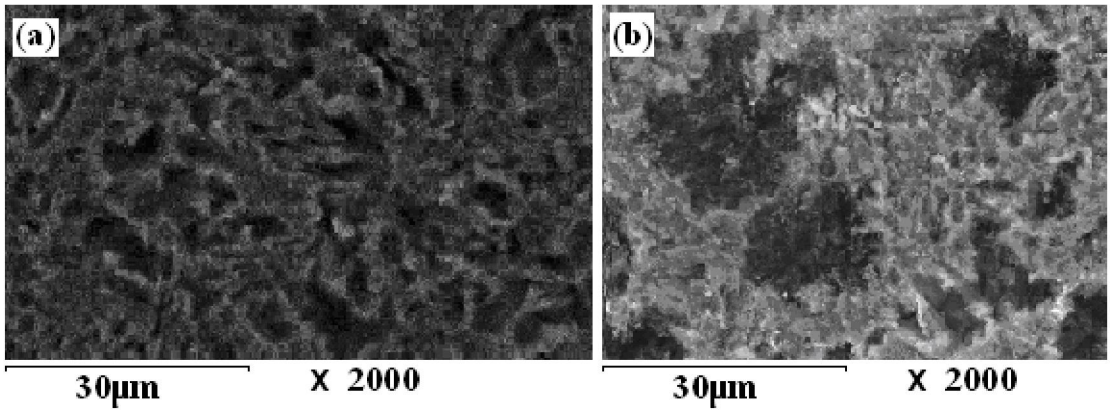

Figure 6: SEM micrograph of the corrosion formed at the surface of Zn electrode after cyclic polarization exposure to (a) 20mmol $(NH_4)_2SO_4$ solution, (b) 20mmol $(NH_4)_2SO_4$ + 25 mmol $(NH_4)_4Ce(SO_4)_4.2H_2O$.

EDX analysis illustrates an intense peak of Zn (Figure 7). As seen, there were many weak peaks for elemental Ce detected. The EDX analysis also detected S- and O- content in the surface which is attributed to the presence of sulfate group in the contact solution.

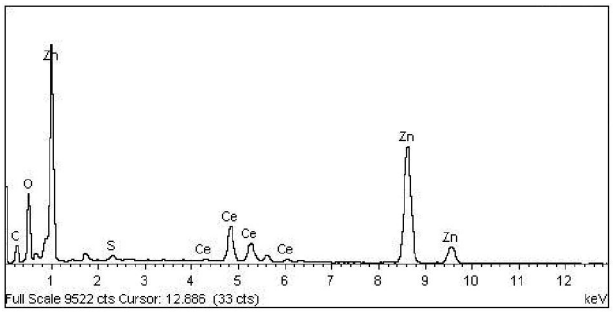

Figure (7): EDX spectra of Zn electrode in 20mmol $(NH_4)_2SO_4$ + 25 mmol $(NH_4)_4Ce(SO_4)_4.2H_2O$.

4- Potentiostatic polarization

The working electrode is kept at a constant potential and the current which flows through the circuit is measured. This constant potential is applied long enough to fully reduce or oxidize all of the substrate in a given solution.

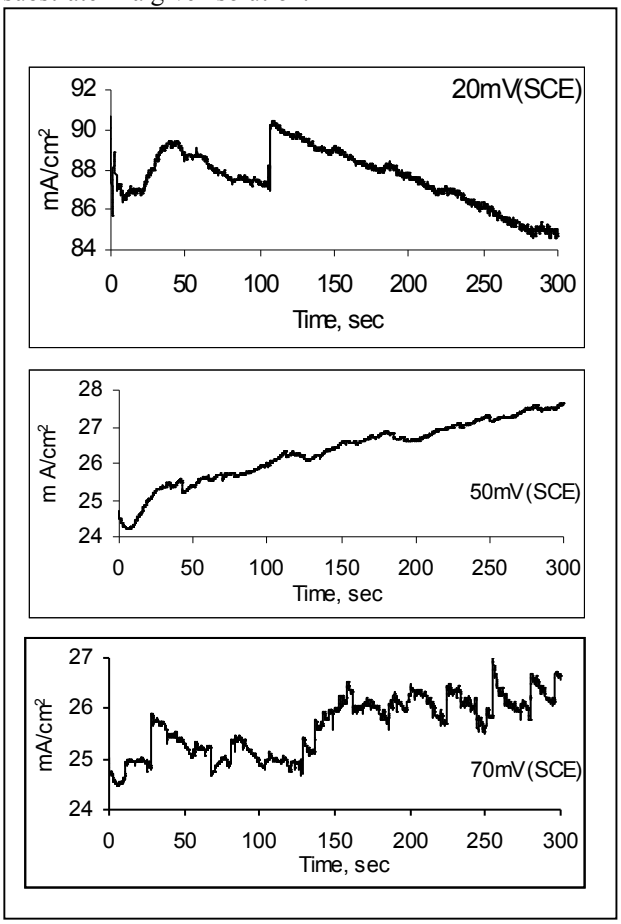

(a)

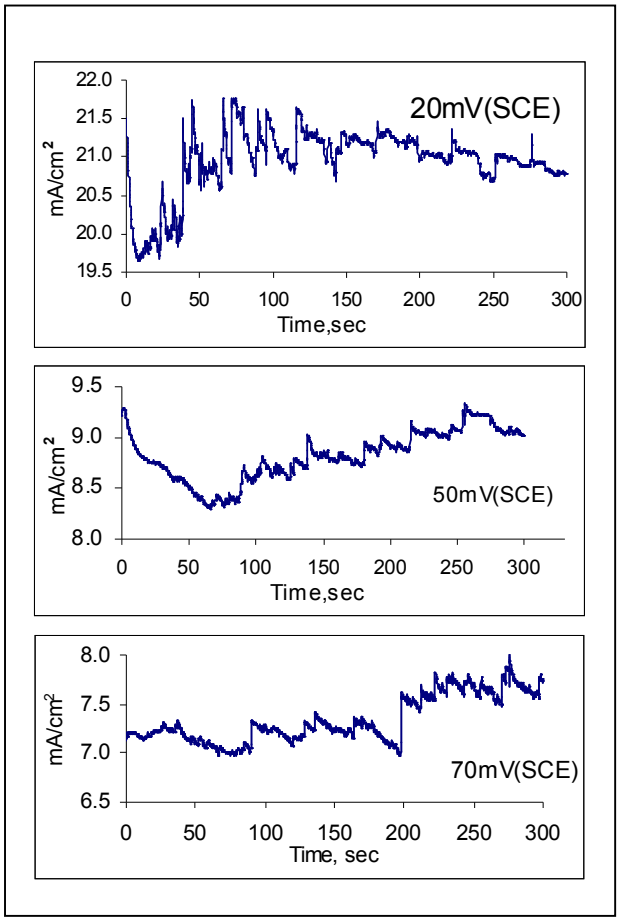

(b)

Figure 8: Potentiostatic polarization curves of Zn electrode at different constant applied potentials (a): in 20mmol $(NH_4)_2SO_4$, (b): in 20mmol $(NH_4)_2SO_4$ + 25 mmol $(NH_4)_4Ce(SO_4)_4.2H_2O$.

In our case, zinc immersed in 20mmol $(NH_4)_2SO_4$ at constant applied potential of 20, 50 and 70 mV/SCE suffers continuous change in current density at all period of time of experiment (Figure 8-a). The instantaneous current densities were decreased with increasing applied potential. For all applied potentials, current density first decreased to a minimum then increased to a top with increasing time in a repetition process in a random way. The decrease of the anodic current coincides with the passivation of zinc electrode; while increasing values coincide with the active dissolution of metal. The repetition of decreasing and increasing of current density values can be attributed to the competition between the anodic formation and chemical dissolution of the passive film on the electrode surface. This means that the stability of the oxide film is affected by the applied

potential. Obviously, the presence of Ce^{+4} ions in $(NH_4)_2SO_4$ solution shifts the current density to more active values compared with values in free $(NH_4)_2SO_4$ solution (Figure 8-b). The later results would be confirmed by the former results from potentiodynamic and cyclic voltammetry that the existence of Ce^{+4} ions in $(NH_4)_2SO_4$ solution enhances Zn corrosion.

5- Surfactants addition

Addition of different concentrations of inhibitors to corrosive solution (20mmol $(NH_4)_2SO_4$ + 25 mmol $(NH_4)_4Ce(SO_4)_4.2H_2O$) at 30°C, shifted the corrosion potential by a value does not exceed ± 20mV(SCE) or ± 7mV(SCE) for inhibitors 17T-HSP or 17T-CM respectively (Figures 9 - 12 and Table 3). Increasing of additive concentration up to 15 mmol lowered the corrosion current densities. This can be correlated with the increasing degree of surface coverage (Θ) due to adsorption of the additive on the zinc surface as the inhibitor concentration was increased. This adsorption depends mainly on the charge and nature of the metal surface, electronic characteristic of the molecules 17T-HSP and 17T-CM and on the electrochemical potential at solution interface [26, 27].

Increasing the concentrations of surfactant 17T-CM in corrosive solution has a slight effect on the cathodic branch associated with the reduction of the metal, and a pronounced inhibitive effect on the anodic branch of the polarization curves during the potential sweep. This indicates that surfactant 17T-CM can be classified as anodic type inhibitor. On the other hand 17T-HSP affected both anodic and cathodic reactions and may be classified as mixed inhibitor.

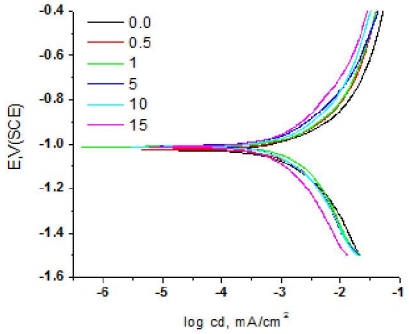

Figure 9: Corrosive solution containing different concentrations of 17T-CM

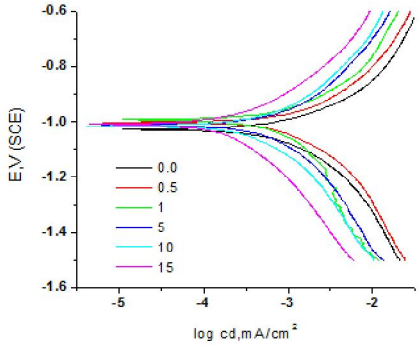

Figure 10: Corrosive solution containing different concentrations of 17T-HSP

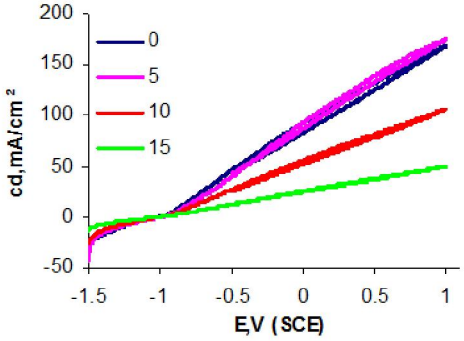

Figure 11: 20mmol $(NH_4)_2SO_4$ + 25 mmol $(NH_4)_4Ce(SO_4)_4.2H_2O$ + different concentrations of 17T-CM

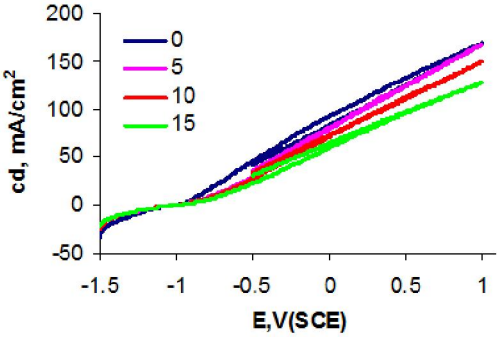

Figure 12: 20mmol $(NH_4)_2SO_4$ + 25 mmol $(NH_4)_4Ce(SO_4)_4.2H_2O$ + different concentrations of 17T-HSP

In the investigated surfactants, the free energy changes of micellization (-7.50, -15.15) and adsorption (-7.64, -15.39) Kcal/mol for 17T-HSP and 17T-CM respectively showed negative sign indicating the spontaneously of the two processes. Also, these surfactants showed higher tendency toward adsorption rather than micellization and the tendency toward adsorption are refereed to the interaction between the aqueous phases and the hydrophobic chains which pumps the surfactant molecules to the interface [18].

Inhibition efficiencies IE% for different concentrations of two surfactants 17T-HSP and 17T-CM as a function of log C_{inh}, increased with rising inhibitor concentration (Figure 13). At low concentrations, the monomers of inhibitors adsorbed at the surface individually with a low percent coverage. As the concentration increases, the amount adsorbed increased leading to a higher degree of coverage and consequently higher corrosion inhibition.

Increasing the maximum surface excess values for 17T-HSP ($3.50x10^{-10}$) rather than 17T-CM ($1.98x10^{-10}$) indicates the increasing of adsorbed molecules at the interface, hence the area available for each molecule will decrease [18]. That causes the compacting of surfactant molecules at the interface to form denser layer, subsequently the adsorption was enhanced in presence of 17T-HSP. The extent of adsorption of different inhibitors depend upon the number of active centers such as N, S, O atoms and the intensities of the type of the hydrophilic group which in this study is effective in 17T-HSP than that in 17T-CM but it cannot provide high corrosion inhibition efficiency for zinc.

Table (3): Electrochemical parameters of Zn electrode in corrosive solution containing different concentrations of additives 17T-HSP and 17T-CM at 5 mV/s and 30°C.

	Type of additive	Conc., mmol	E_{corr} mV	R_p Ωcm^2	I_{corr} mA/cm^2	b_a mV/decade	b_c mV/decade	C_R mm/y
potentiodynamic		Blank	-1015	32.75	1.7286	258	-419	20.21
	17T-HSP	0.5	-1003	36.12	0.8612	155	-217	10.07
		1	-994	56.21	0.8475	184	-353	9.912
		5	-1019	65.62	0.7724	242	-342	9.034
		10	-1022	92.00	0.5799	229	-345	6.782
		15	-1016	182.59	0.2410	190	-317	2.819
	17T-CM	0.5	-1013	32.63	1.5174	236	-370	17.74
		1	-1030	42.25	1.3427	225	-349	15.70
		5	-1012	43.46	1.1818	241	-345	13.82
		10	-1008	48.91	0.8915	220	-279	10.42
		15	-1019	65.62	0.7724	242	-342	9.034
Cyclic voltametric		Blank	-1024	29.97	1.354	189	-292	15.83
	17T-HSP	5	-1015	47.24	0.9519	209	-280	11.13
		10	-1011	53.29	0.9248	248	-286	10.81
		15	-1014	54.43	0.8012	187	-253	09.37
	17T-CM	5	-999	38	1.2477	194	-281	14.60
		10	-1004	37.14	1.208	213	-294	14.13
		15	-1020	70.66	0.749	256	-310	08.76

E_{corr}, corrosion potential I_{corr}, corrosion current density b_a, anodic Tafel slope b_C, cathodic Tafel slope C_R, corrosion rate.

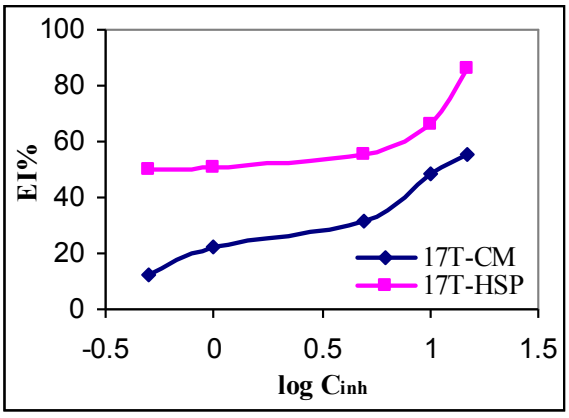

Figure 13: The relationship between inhibition efficiency IE % and Log C_{inh}.

Low IE% values indicated that the interaction responsible for bonding of inhibitors to a metal surface was weak undirected interaction which might be due to electrostatic attraction between inhibiting surfactant ions and the electrically charged surface of metal [26, 28].

As can be seen from Figure 14(a), the surface of zinc electrode in the presence of 17T-HSP containing solution is covered by denser protective gelatinious layer compared with that in the solution without additive (Figure 6 b). Differently, the covered layer in the 17T-CM containing solution is rock-like as shown in Figure 15(a). The difference in molecular structure, sulfonate for 17T-HSP and carboxylate for 17T-CM, contributes to the different adsorption mechanism. The respective EDX spectrum for each inhibitor is free from elemental cerium which is very effective in the corrosion process (Figures14(b) and 15(b)).

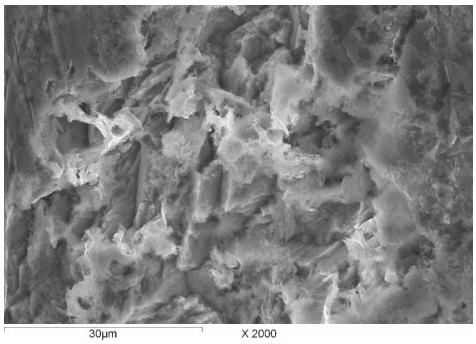

Figure 14: (a) SEM and (b) EDX micrograph of the layer formed at the surface of Zn electrode after cyclic polarization in a corrosive solution containing 15 mmol 17T-HSP

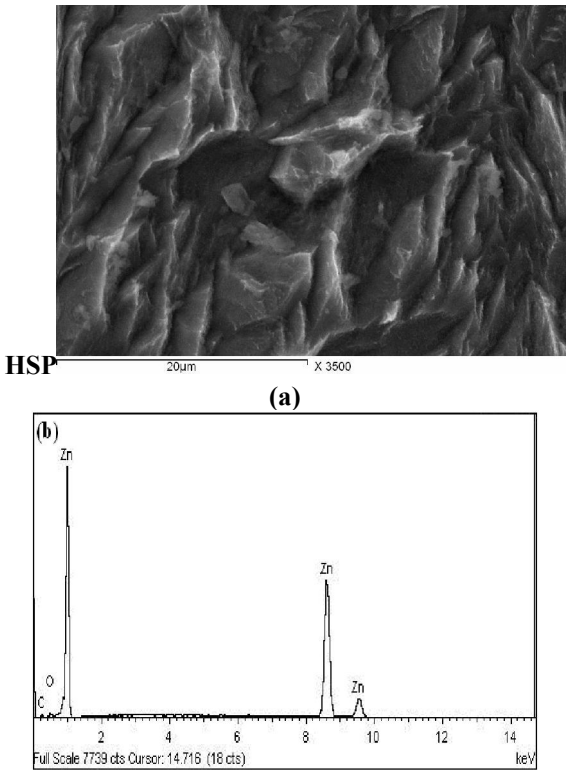

Figure 15: (a) SEM and (b) EDX micrograph of the layer formed at the surface of Zn after cyclic polarization in a corrosive solution containing 15 mmol 17T-CM

However, to quantify the effect of inhibitor concentration on the corrosion rate theoretical fitting of different isotherms are tested.

Adsorption isotherms

1- Langmuir isotherm

The Langmuir equation was chosen for the estimation of maximum adsorption capacity corresponding to complete monolayer coverage on the adsorbent surface. A form of the Langmuir model is [29]:

$$C_{inh}/\Theta = 1/K_{ads} B_s + C_{inh}/B_s \quad (12)$$

where C_{inh}, is the molar inhibitor concentration, Θ, is the surface coverage by inhibitor molecules, B_s, is the sorbent binding capacity (mmol/mol), and K_{ads} (L mol^{-1}), is the binding constant which is defined as [11, 30]:

$$K_{ads} = \frac{1}{55.5} \exp\left(\frac{-\Delta G_{ads}}{RT}\right) \quad (13)$$

Where R, is the universal gas constant, 8.314 J/mol K, T is the absolute temperature and ΔG_{ads}, is the adsorption free energy.

Plots of C_{inh}/Θ versus surfactant concentration are illustrated in Figure 16. The regression coefficient (R^2) and the different constants for this model are given on Table (4). This model gave a poor fit to the experimental data for 17T-HSP due to its low regression coefficient value. This agrees with the transition found in figure 13, which could be owing to the change from traditional submonolayer level Langmuir adsorption to multilayer adsorption [26]. On the other hand different constants for 17T-CM indicate a good fit of the isotherm to the experimental data which reflects monolayer adsorption. The negative and low values of ΔG_{ads} indicate the spontaneous and physical nature of adsorption [31, 32].

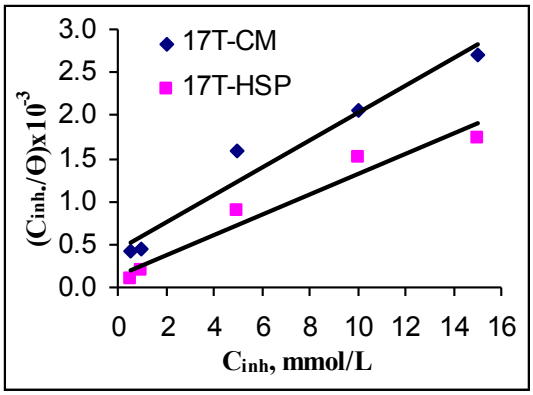

Figure 16: Dependence of C_{inh}/Θ on the concentration of inhibitor in corrosive solution at 30°C.

2- Freundlich isotherm

Application of the Freundlich equation to analyze the equilibrium isotherms of the two additives gave linear plots (Figure 17). The linearized form is given as [31]:

$$\log \Theta = \log K_{ads} + 1/n \log C_{inh} \quad (14)$$

Where, K_{ads} (the binding constant) and n (the exponent) are the Freundlich empirical constants, C_{inh} is the additive concentration (mol/L) and Θ is the surface coverage. The values of K_{ads} and n determine the steepness and curvature of the isotherm [33].

The values of 1/n, less than unity (Table 4) is an indication of that a significant adsorption takes place at low concentration but the increase in the amount adsorbed with concentration becomes less significant at higher concentrations and vice verse [34]. Also, the higher the K_{ads} value, the greater the adsorption intensity. In the present study, this model gave a very good description of the sorption process over the range of concentrations studied.

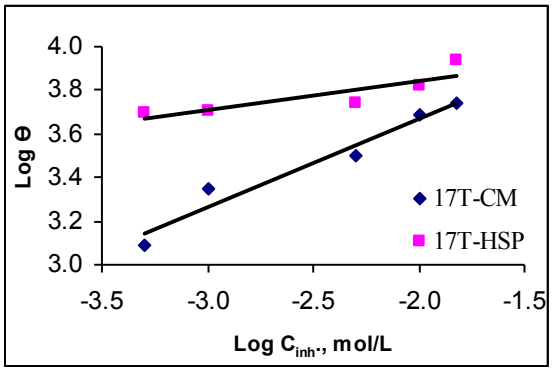

Figure 17: Freundlich isotherm plots for 17T-CM and 17T-HSP of different concentrations in corrosive solution at 30°C on zinc surface.

Table (4): Regression coefficient of determination (R^2) and the different constants for Langmuir and Freundlich isotherm models for the surfactants 17T-CM and 17T-HSP adsorption on zinc surface

	17T-CM	17T-HSP
Langmuire isotherm		
R^2	0.9587	0.7496
B_s	5000	$5x10^7$
K_{ads}	500	200
ΔG_{ads}, $kJmol^{-1}$	-25.73	-23.42
Freundlich isotherm		
R^2	0.9552	0.9522
K_{ads}	1835	5163
1/n	0.4063	0.1334
n	2.46	7.49

Conclusion

Increasing $(NH_4)_2SO_4$ concentrations induce the corrosion of Zn. While increasing the scan rate has no effect on the corrosion process. Potentiostatic, potentiodynamic and cyclic voltametric techniques ensures that combined effect of $(NH_4)_4Ce(SO_4)_4.2H_2O$ and $(NH_4)_2SO_4$ on Zn electrode accelerate the zinc corrosion more than that in $(NH_4)_2SO_4$ alone.

Surfactant 17T-CM is a weak anodic inhibitor, whereas 17T-HSP is a weak mixed inhibitor for Zn in corrosive solution. The difference in molecular structure contributes to the different adsorption mechanism.

References

1. Jia Z., D.R. Zhou, C.F. Zhang; Trans. Nonferr. Met. Soc. China 15 (2005) 15.
2. Qu Q., L. Li, W. Bai, C-W Yan, C-N Cao;. Corros. Sci. 47 (2005) 2832.
3. Uranaka M. and T.Shimizu;.Metallurgical Science and Technology. 30(2012)30.
4. Santana J.J., B.M. Fernández-Pérez, J. Morales, H.C. Vasconcelos, R.M. Souto, and S. González;Int. J. Electrochem. Sci., 7 (2012) 12730.
5. Assafa F.H., S.S. Abd El-Rehiem, A.M. Zakya; Mater. Chem. Phys. 58 (1999) 58.
6. SZŁAPA I., D.JĘDRZEJCZYK, M.HAJDUGA, S.WĘGRZYNKIEWICZ and D.SOŁEK;. Brno, Czech Republic, EU.5(2013)15
7. Qu Q., L. Li, W. Bai, C-W Yan; Trans. Nonferr. Met. Soc China 16(2006) 887.
8. Sanyal B., D.V. Bhadwar;. J. Sci. Ind. Res. 21D (1962) 243.
9. Lindström R., J.E. Svensson, L.G. Johansson; J. Electrochem. Soc. 149 (2002) B57.
10. Aramaki K.; Corros. Sci. 44 (2002) 1361.
11. Foad E.E. El Sherbini, S.S. Abd El Rehim; Corros. Sci. 42 (2000) 785.
12. H. Zhou, Q. Huang, M. Liang, D. Lv, M. Xu, H. Li, W. Li; Mater. Chem. Phys. 128 (2011) 214.
13. Attia E. M., F. H. Abd EL- Salam; Al-Azhar Bull. Sci. 20 (2009) 43.
14. Moura E. F., A. O. W. Neto, T. N. C. Dantas, H. S. Júnior, A. Gurgel; Collo. Surf. A: Physicochem. Eng. Asp. 340 (2009) 199.
15. Vittal R., H. Gomathi, K-J Kim; A. Collo. Interf. Sci. 119(2006)55.
16. Chebabe D., Z.A. Chikh, N. Hajjaji, A.A. Srhiri, F. Zucchi; Corros. Sci. 45 (2003) 309.
17. Qiu L-G, A-J Xie, Y-H Shen; Mater. Chem. Phys. 91 (2005) 269.
18. Abd El-Salam F. H.; J. Disp. Sci.Tech. 31(2010)1362.
19. Sziráki L., À. Gziráki, I. Geröcs, Z. Vértesy, L. Kiss; Electrochim. Acta 43(1998) 175.

20. Veleva L., M. Acosta, E. Meraz; Corros. Sci. 51 (2009) 2055.
21. El-Mahdy G.A., K.B. Kim; Corros. 61 (2005) 420.
22. P.W. ATKINS; Physical Chemistry Atkins, pp. 948 6th ed. Oxford (1998).
23. Hanna E.M., A. D. Pethybridge, J. E. Prue; Electrochim. Acta 16(1971) 677.
24. Li X., S. Deng, H. Fu, G. Mu, N. Zhao; Appl. Surf. Sci. 254 (2008) 5574.
25. Li X.H., S.D. Deng, G.N. Mu, Q. Qu; Mater. Lett. 61 (2007) 2514.
26. Attia E. M.; Al-Azhar Bull. Sci. 19 (2008) 135.
27. I. L. Rozendeld; Corrosion Inhibitors, McGraw-Hill, New York, NY (1981) p. 327.
28. Quartarone G., L. Bonaldo, C. Tortato; Appl. Surf. Sci. 252 (2006) 8251.
29. Huichao G., L. Wenjun, W. Huanying, Z. Jinghua, L. Yang, Z. Yue; Rare Metals 30 (2011) 58.
30. Qiu L-G, Y. Wu, Y-M Wang, X. Jiang; Corros. Sci. 50 (2008)576.
31. Attia E. M., Z. A. EL- Shafiey; Al-Azhar Bull. Sci. 20 (2009) 23.
32. Prabhu R.A., T.V. Venkatesha, A.V. Shanbhag, G.M. Kulkarni, R.G. Lalkhambkar; Corros. Sci. 50 (2008) 3356.
33. Igwe J. C., A. A. Abia; Electron. J. Biotechnol. 10 (2007)536.
34. Teng H., C. Hsieh; Ind. Eng. Chem. Res. 37 (1998) 3618.

12/26/2013